Hydrogen Evolution Reaction

International Edition: DOI: 10.1002/anie.201906134
German Edition: DOI: 10.1002/ange.201906134

Boosting Electrocatalytic Hydrogen Evolution over Metal–Organic Frameworks by Plasmon-Induced Hot-Electron Injection

Shan-Shan Wang[+], Long Jiao[+], Yunyang Qian, Wen-Chao Hu, Gui-Yin Xu, Chen Wang, and Hai-Long Jiang**

Abstract: *Efficient hydrogen evolution via electrocatalytic water splitting holds great promise in modern energy devices. Herein, we demonstrate that the localized surface plasmon resonance (LSPR) excitation of Au nanorods (NRs) dramatically improves the electrocatalytic hydrogen evolution activity of CoFe-metal–organic framework nanosheets (CoFe-MOFNs), leading to a more than 4-fold increase of current density at −0.236 V (vs. RHE) for Au/CoFe-MOFNs composite under light irradiation versus in dark. Mechanistic investigations reveal that the hydrogen evolution enhancement can be largely attributed to the injection of hot electrons from AuNRs to CoFe-MOFNs, raising the Fermi level of CoFe-MOFNs, facilitating the reduction of H_2O and affording decreased activation energy for HER. This study highlights the superiority of plasmonic excitation on improving electrocatalytic efficiency of MOFs and provides a novel avenue towards the design of highly efficient water-splitting systems under light irradiation.*

Hydrogen is one of the most promising energy carriers. Electrochemical water splitting has been regarded as one of the most efficient and sustainable strategies for hydrogen generation.[1] Although precious metals are efficient for hydrogen evolution reaction (HER),[1] their scarcity and high cost limit the practical utilization. Huge efforts have been devoted to fabricate efficient non-noble-metal electrocatalysts in both homogeneous and heterogeneous systems. Generally, homogeneous catalysts show well-defined structures favorable to mechanistic studies while suffering from poor recoverability. In contrast, heterogeneous catalysts are easily recyclable and potentially cost-effective, while the number and location of active centers on solid catalyst surfaces are often indistinct and prone to change under reaction environments making mechanistic studies difficult.

Metal–organic frameworks (MOFs), with porous structures built from metal ions/clusters and organic ligands, have presented many advantages for catalysis.[2] Similar to molecular catalysts, MOFs possess well-defined structures and readily accessible active sites. Meanwhile, MOFs are solid porous materials and thus recyclable. The unique features of MOFs make them ideal candidates to integrate the inherent advantages of both homogeneous and heterogeneous catalysts.[3] Up to now, very limited MOFs show high HER activity,[4] among which 2D MOF nanosheets are very promising for enhanced electrocatalysis.[5] Although substantial progress has been achieved, more effective strategies are still needed to be developed to enhance the electrocatalytic HER performance of MOFs.

Localized surface plasmon resonance (LSPR), the collective oscillation behavior of conduction electrons of noble metals driven by incident light, could offer metal nanoparticles several unique benefits including the enhanced local electromagnetic fields, efficient charge-carrier separation and the heat effect during the photon dissipation.[6] Recently, it is found that the LSPR effect can also accelerate the electrochemical processes by the injection of hot electrons.[7] Thus, the introduction of plasmonic effect into MOFs could be an effective method to boost the overall electrocatalytic processes.

With all the above in mind, a plasmon-enhanced HER electrochemical system based on the assembly of Au nanorods (AuNRs) and 2D CoFe-MOF nanosheets (CoFe-MOFNs), was rationally constructed to afford Au/CoFe-MOFNs composite (Scheme 1). The AuNRs, as a light absorber and plasmon exciter, can generate hot electrons upon irradiation. The 2D CoFe-MOFNs, with highly exposed active sites, were chosen as the HER electrocatalysts. Under light irradiation, the HER activity of Au/CoFe-MOFNs can

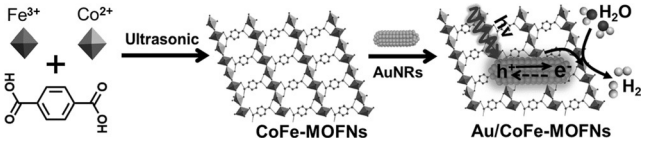

Scheme 1. Illustration of the synthesis of Au/CoFe-MOFNs and the experimental principle of enhanced HER activity.

[*] S. S. Wang,[+] W. C. Hu, Prof. Dr. C. Wang
Key Laboratory of Biomedical Functional Materials
School of Science, China Pharmaceutical University
Nanjing, Jiangsu 211198 (China)
E-mail: wangchen@cpu.edu.cn
L. Jiao,[+] Y. Qian, Prof. Dr. H.-L. Jiang
Hefei National Laboratory for Physical Sciences at the Microscale, Collaborative Innovation Center of Suzhou Nano Science and Technology, Department of Chemistry
University of Science and Technology of China
Hefei, Anhui 230026 (China)
E-mail: jianglab@ustc.edu.cn
Homepage: http://staff.ustc.edu.cn/~jianglab/
Dr. G. Y. Xu
Department of Nuclear Science and Engineering, Massachusetts Institute of Technology
Cambridge, MA 02139 (USA)
[+] These authors contributed equally to this work.
Supporting information and the ORCID identification number(s) for the author(s) of this article can be found under: https://doi.org/10.1002/anie.201906134.

be significantly enhanced (approximately 4-fold enhancement at −0.236 V) by hot-electron injection from AuNRs into the MOF. Mechanistic investigations found that charge transfer can raise the Fermi level of the MOF, making it match better with the H_2O/H_2 potential and thus offering significantly decreased activation energy for HER.

The 2D CoFe-MOFNs were synthesized from a mixed solution of Co^{2+}, Fe^{3+} and benzenedicarboxylic acid (BDC) through a simple ultrasonic method.[5] The CoFe-MOFNs with a sheet-like structure could be clearly observed by scanning electron microscopy (SEM), transmission electron microscopy (TEM) and the atomic force microscopy (AFM) images (Figure 1 a, Figure S1 in the Supporting Information).

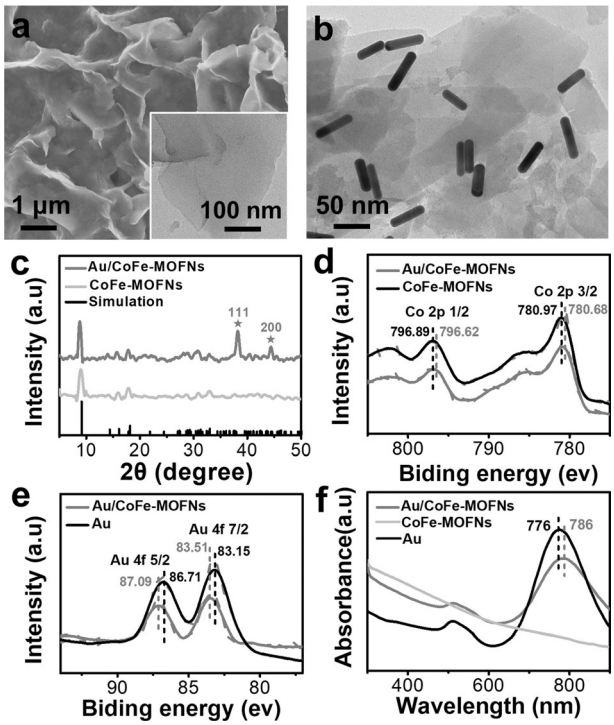

Figure 1. a) SEM image of the prepared CoFe-MOFNs (Inset: TEM image). b) TEM image of Au/CoFe-MOFNs composite. c) XRD patterns of Au/CoFe-MOFNs composite and CoFe-MOFNs. d) The Co 2p and e) Au 4f XPS spectra of Au/CoFe-MOFNs composite and AuNRs, CoFe-MOFNs. f) UV/Vis absorption spectra of Au/CoFe-MOFNs composite, CoFe-MOFNs and AuNRs.

AuNRs of approximately 52 nm long and 12 nm wide were then synthesized and assembled onto the CoFe-MOFNs to afford AuNRs/CoFe-MOFNs with 2.2 wt % Au loading (Figure 1 b, Figure S2). TEM observation of the composite reveals that AuNRs are randomly decorated on the surface of CoFe-MOFNs (Figure 1 b). Powder X-ray diffraction (XRD) patterns of CoFe-MOFNs and Au/CoFe-MOFNs well match with that of the simulated MOF, demonstrating the retained crystallinity of CoFe-MOFNs after the furnishing of AuNRs (Figure 1 c). In addition, the characteristic peaks at 38.17° and 44.46° assigned to Au (111) and Au (200) can be observed in Au/CoFe-MOFNs (Figure 1 c), indicating the incorporation of AuNRs. Zeta potentials of CoFe-MOFNs and AuNRs in aqueous solution were measured to be −10.21 mV and +37.5 mV, respectively, indicating that they are able to contact closely via electrostatic interaction (Figure S3), which would be beneficial to electron transfer between them.[8]

The X-ray photoelectron spectroscopy (XPS) spectra show that the binding energies of Co $2p_{1/2}$ and Co $2p_{3/2}$ in Au/CoFe-MOFNs are negatively shifted by approximately 0.27 and 0.29 eV respectively, as compared to those in CoFe-MOFNs (Figure 1 d). Meanwhile, the binding energies of Au $4f_{5/2}$ and Au $4f_{7/2}$ in Au/CoFe-MOFNs are positively shifted by approximately 0.38 and 0.36 eV respectively compared to those for AuNRs (Figure 1 e). These results unambiguously confirm the electron transfer from AuNRs to CoFe-MOFNs in Au/CoFe-MOFNs.[7c] The Au/CoFe-MOFNs composite presents a strong UV/Vis absorption peak centered at 786 nm (Figure 1 f), which is induced by the surface plasmon excitation of AuNRs. There is an approximately 10 nm red shift in Au/CoFe-MOFNs as compared with the original AuNRs, due to electronic interactions between AuNRs and CoFe-MOFNs, in consistence with the XPS results. The calculated energy levels based on the UV/Vis spectra and cyclic voltammogram (CV) suggest a more negative LUMO level (−0.31 V vs. normal hydrogen electrode; NHE) than H_2O/H_2 potential (Figure S4, S5), supporting the possibility of CoFe-MOFNs to catalyze hydrogen evolution once getting electrons from AuNRs.

Inspired by the results above, electrocatalytic HER over Au/CoFe-MOFNs composite was investigated in a N_2-saturated 0.1 M KOH at 30 °C.[7c] When in dark, the linear sweep voltammetry (LSV) curve of CoFe-MOFNs shows an overpotential of −0.333 V at 1 mA cm^{-2} for HER, much better than Co-MOFNs and Fe-MOFNs (Figure S6). The XPS results indicate the charge transfer from Fe to Co in CoFe-MOFNs, resulting in favorable proton reduction on Co sites (Figure S7). The electrochemical measurements illustrate the much smaller charge-transfer resistance and much higher electrochemical surface area (ECSA) of CoFe-MOFNs than Co-MOFNs and Fe-MOFNs (Figure S8, S9). Furthermore, DFT calculations reveal that Co sites in CoFe-MOFNs present the smallest ΔG_{H^*} among all metal sites in Fe-MOFNs, Co-MOFNs and CoFe-MOFNs (Figure S10–12). All these results clearly elucidate the superior HER process of CoFe-MOFNs.

Upon integrating AuNRs and CoFe-MOFNs, the resultant Au/CoFe-MOFNs composite exhibits much higher HER activity than the pure CoFe-MOFNs and AuNRs with an onset potential of around −0.228 V versus the reversible hydrogen electrode (RHE), indicating enhancement effect due to charge interaction between AuNRs and CoFe-MOFNs (Figure 2 a,b).[9] When irradiated with an 808 nm laser (corresponding to the maximum LSPR absorption of AuNRs), the HER activity of Au/CoFe-MOFNs is considerably enhanced, presenting a much lower onset potential (ca. −0.135 V vs. RHE) and much higher current increase rate than that in dark (Figure 2 a,b). In contrast, different counterpart catalysts, including CoFe-MOFNs, AuNRs, Au/Co-MOFNs and Au/Fe-MOFNs, Au/Ni-MOFNs, Au/CoNi-MOFNs, Au/NiFe-MOFNs, Au nanospheres (AuNSPs)/CoFe-MOFNs and Au nanostars (AuNSs)/CoFe-MOFNs exhibit much weaker light

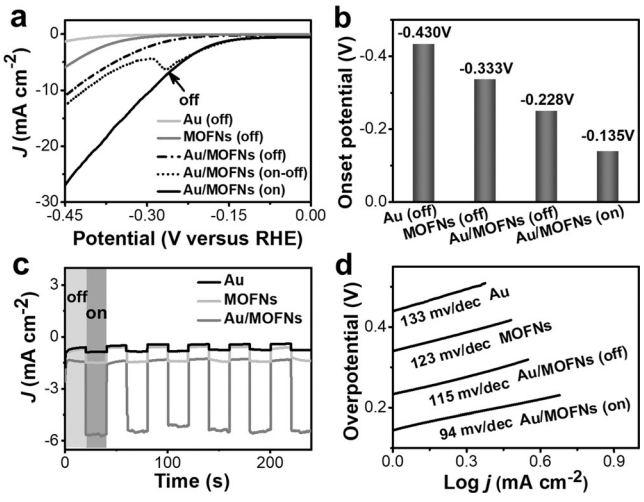

Figure 2. a) HER polarization curves, b) onset potentials, c) *I–t* curves and d) the Tafel plots of AuNRs, CoFe-MOFNs, Au/CoFe-MOFNs in the absence or presence of light irradiation. To save space, the CoFe-MOFNs is marked as MOFNs in the figures.

response under identical irradiation conditions (Figure S13–S18).

To further verify such instant photoresponse of Au/CoFe-MOFNs, a LSV scanning with light on and off was also performed. An abrupt drop in current is observed when the light is removed at around −0.260 V (Figure 2a). Interestingly, the current of Au/CoFe-MOFNs does not immediately return to the original state with light off, which might be caused by photothermal effect and roughly evaluated to be about 33% of total LSPR effect (Figure S19). Then, the chronoamperometric curve of Au/CoFe-MOFNs at around −0.236 V under chopped illumination was collected (Figure 2c). It can be seen that Au/CoFe-MOFNs exhibits prompt and reproducible current responses to on-off illumination cycles. In contrast to Au/CoFe-MOFNs, CoFe-MOFNs or AuNRs show negligible current improvement under irradiation and the slight increase could be due to thermal effect around the electrode. The results reveal that the integration of AuNRs and CoFe-MOFNs is indispensable for the photoenhancement effect. To further illustrate the superiority of 2D structure of CoFe-MOFNs, bulk CoFe-MOF has been synthesized and integrated with AuNRs. The obtained Au/bulk CoFe-MOF shows much inferior HER performance to the Au/CoFe-MOFNs (Figure S20), clearly highlighting the structure advantage of Au/CoFe-MOFNs.

Based on the polarization curves in Figure 2a, the corresponding Tafel plots are further calculated to evaluate the influence of light irradiation on the HER kinetics. It can be seen that Au/CoFe-MOFNs shows a Tafel slope of 115 mV/dec in the dark. Delightedly, with 808 nm laser irradiation, the Tafel slope of Au/CoFe-MOFNs is significantly decreased to 94 mV/dec. This clearly indicates the accelerated HER kinetics by light-induced LSPR of AuNRs (Figure 2d). Electrochemical impedance spectroscopy (EIS) plots of Au/CoFe-MOFNs with and without laser irradiation indicate that the plasmon excited "hot electrons" cause a higher charge transport efficiency in the electrode (Figure S21).

The HER activity of both Au/CoFe-MOFNs and the MOF can also be improved under full spectrum light irradiation (Figure S22). However the enhancement is the highest under 808 nm illumination, in accordance with the previous report.[6c] To further confirm the contribution of photogenerated hot electrons of AuNRs to HER performance, excitation-wavelength-dependent HER activity of Au/CoFe-MOFNs was measured (Figure 3a, Figure S23). It can be seen

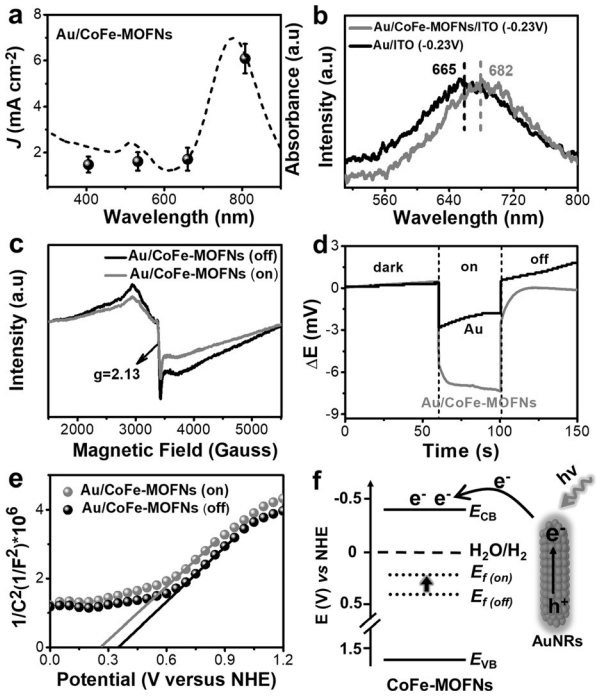

Figure 3. a) Current density of Au/CoFe-MOFNs composite with different wavelengths. b) LSPR scattering spectra of AuNRS in Au/ITO and Au/CoFe-MOFNs/ITO at −0.23 V vs. RHE in 0.1 M KCl solution. c) EPR spectra of Au/CoFe-MOFNs composite with light on and off. d) Chronopotentiometry of the V_{oc} from Au/CoFe-MOFNs composite and AuNRs under 808 nm irradiation. e) Mott–Schottky plots of Au/CoFe-MOFNs with light off and on at a frequency of 1000 Hz. f) Schematic and energy level diagram illuminating hot-electron injection from AuNRs to CoFe-MOFNs.

that the current densities at −0.250 V under different wavelengths show a similar profile to the absorbance of Au/CoFe-MOFNs. We therefore can ascribe the light enhanced HER activity to the LSPR effect of AuNRs.[10] In addition, we also observed that the HER activity of Au/CoFe-MOFNs dramatically increased with the illumination intensity up to approximately 1500 mW cm^{-2} (Figure S24). The linear dependence is a signal of hot-electron-driven chemical process.[10,11] Furthermore, starting from a relatively low Au loading (0.5 wt%), the HER activity of Au/CoFe-MOFNs improves with increased Au loadings, while the activity decreases when Au loading is higher than 2.2 wt%, manifesting the optimal Au loading and volcano-type curve (Figure S25).

Hot electrons upon LSPR excitation are assumed to have varied possible transfer channels (Figure S26). To obtain direct evidence of hot electron injection, the dark field spectroscopy experiments have been conducted (Fig-

ure S27, S28) and the LSPR scattering peak locates at 665 nm, which undergoes a red-shift to 682 nm after the assembly of CoFe-MOFNs (Figure 3b). The red shift indicates a reduced electron density on AuNR surface,[7a] which is caused by the fast hot electron injection from AuNR to CoFe-MOFNs. Electron paramagnetic resonance (EPR) spectrum for Au/CoFe-MOFNs shows a clear signal ($g = 2.13$) assignable to Co^{2+} (Figure 3c).[12] Upon exposure to 808 nm light, the weakened Co^{2+} signal indicates partial reduction of Co^{II} to Co^{I}. In contrast, almost no change can be observed in the EPR spectrum of pure CoFe-MOFNs after light irradiation (Figure S29). These results well demonstrate the hot electrons injection from excited AuNRs to Co^{II} in Au/CoFe-MOFNs. In addition, the open-circuit photovoltage (V_{oc}) decay (OCPVD) measurement was further carried out (Figure 3d). The potential of Au/CoFe-MOFNs has the more negative shift, correlating to the Fermi level shift toward more negative potentials, which indicates an improved charge transfer from AuNRs to CoFe-MOFNs and electron accumulation in the AuNRs/CoFe-MOFNs heterojunctions.[13] The continuous electron transfer from AuNRs to the MOF would lead to the shift of Fermi level (E_f), which can be investigated from the Mott–Schottky plots (Figure 3e). The positive slope indicates n-type semiconductor character of CoFe-MOFNs.[14] The flat potential (equal to E_f for n-type semiconductor[15]) determined to be 0.356 (vs. NHE) in the dark, while it is reduced to 0.261 V (vs. NHE) under light irradiation. It is clear that, upon light irradiation, the Fermi level of CoFe-MOFNs is raised to be more comparable to the energy level for redox pair H_2O/H_2 potential (0 V) (Figure 3f), which would then reduce the overpotential of CoFe-MOFNs for HER and thus an enhanced HER performance can be expected.[7c,14]

To gain more evidence for the LSPR enhanced HER activity of Au/CoFe-MOFNs, the activation energies (E_a) of HER with light on and off were further performed to provide quantitative insights into the energetics (Figure 4a, Figure S30).The HER reaction rates, under both light irradiation and dark, can be promoted with elevated temperatures. Plot of $\ln j$–$1/T$ (j: current density; T: temperature) results in linear lines (Figure 4a, inset), showing the typical Arrhenius behavior. Using Arrhenius equation and kinetic data, the value of E_a for Au/CoFe-MOFNs in dark is calculated to be 113.55 kJ mol^{-1}. After irradiation with 808 nm laser, the E_a decreases to 63.24 kJ mol^{-1} (Figure 4b). As a result, a decrease of 50.31 kJ mol^{-1} in reaction activation energy resulting from the plasmonic activation under 808 nm irradiation can be concluded (Figure 4c). The decreased activation energy originates from direct hot-electron injection from plasmonic AuNRs to CoFe-MOFNs, leading to upraised energy level of the MOF. Furthermore, the higher light excitation power, the lower activation energy can be observed. The apparent activation energy decreased until the effect began to taper off at the highest power explored in this work (Figure 4d), suggesting that the photo-assisted reaction is mainly owing to the electron transfer effect.[10]

In conclusion, plasmonic AuNRs stabilized on CoFe-MOFNs have been constructed as an electrocatalyst for much enhanced HER performance by LSPR excitation. Upon light irradiation, the overpotential at a current density of 1 mA cm^{-2} decreases from 228 to 135 mV and current density realizes an approximately 4-fold (at −0.236 V) enhancement. As evidenced by photoelectrochemical analysis and EPR results, this enhanced activity relies on the efficient injection of hot electrons from plasmonic AuNRs to CoFe-MOFNs under light irradiation. This charge transfer results in a raised Fermi level of CoFe-MOFNs to match better with the energy level of H_2O/H_2 potential. In addition, the HER activation energy is significantly decreased due to the LSPR effect under light irradiation and thus the HER process can be driven more easily. To our knowledge, this is the first report on the integration of the plasmonic effect into MOFs for enhanced HER. It is believed that the findings provide new avenues to design and fabrication of efficient, yet simple, water splitting systems.

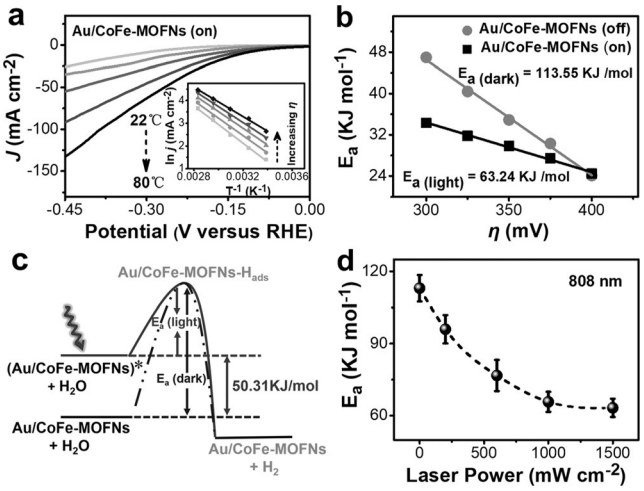

Figure 4. a) HER activity of Au/CoFe-MOFNs composite under 808 nm laser excitation at different temperatures (Inset: Arrhenius plots). Overpotentials are taken from 250 to 400 mV at an interval of 50 mV. b) Activation energy with light off and on at the zero overpotential obtained through trend extrapolation. c) Schematic representation of the activation energy change of Au/CoFe-MOFNs composite by 808 nm irradiation. d) Activation energy change of Au/CoFe-MOFNs composite irradiated by laser with different intensities.

Acknowledgements

This work was supported by the NSFC (21575163, 21874155, 21725101, 21673213, 21871244, 21521001), Double First-Class University project (CPU2018GY25) and Fujian Institute of Innovation (CAS).

Conflict of interest

The authors declare no conflict of interest.

Keywords: electrocatalysis · gold nanorods · hydrogen evolution reaction · metal–organic frameworks · plasmons

How to cite: *Angew. Chem. Int. Ed.* **2019**, *58*, 10713 – 10717
Angew. Chem. **2019**, *131*, 10823 – 10827

[1] a) X. X. Zou, Y. Zhang, *Chem. Soc. Rev.* **2015**, *44*, 5148 – 5180; b) I. Roger, M. A. Shipman, M. D. Symes, *Nat. Rev. Chem.* **2017**, *1*, 0003; c) Y. Li, H. Wang, L. Xie, Y. Liang, G. Hong, H. Dai, *J. Am. Chem. Soc.* **2011**, *133*, 7296 – 7299; d) Y. Tan, H. Wang, P. Liu, Y. Shen, C. Cheng, A. Hirata, T. Fujita, Z. Tang, M. Chen, *Energy Environ. Sci.* **2016**, *9*, 2257 – 2261; e) L. Fan, P. F. Liu, X. Yan, L. Gu, Z. Z. Yang, H. G. Yang, S. Qiu, X. Yao, *Nat. Commun.* **2016**, *7*, 10667; f) Y. Zheng, Y. Jiao, A. Vasileff, S. Z. Qiao, *Angew. Chem. Int. Ed.* **2018**, *57*, 7568 – 7579; *Angew. Chem.* **2018**, *130*, 7690 – 7702.

[2] a) H. Furukawa, K. E. Cordova, M. O'Keeffe, O. M. Yaghi, *Science* **2013**, *341*, 1230444; b) H. C. Zhou, S. Kitagawa, *Chem. Soc. Rev.* **2014**, *43*, 5415 – 5418; c) Z. Liang, C. Qu, W. Guo, R. Zou, Q. Xu, *Adv. Mater.* **2018**, *30*, 1702891; d) B. Li, H. M. Wen, Y. Cui, W. Zhou, G. Qian, B. Chen, *Adv. Mater.* **2016**, *28*, 8819 – 8860; e) Q. Yang, Q. Xu, H. L. Jiang, *Chem. Soc. Rev.* **2017**, *46*, 4774 – 4808.

[3] a) G. Li, S. Zhao, Y. Zhang, Z. Tang, *Adv. Mater.* **2018**, *30*, 1800702; b) L. Jiao, Y. Wang, H. L. Jiang, Q. Xu, *Adv. Mater.* **2018**, *30*, 1703663; c) J. D. Xiao, H. L. Jiang, *Acc. Chem. Res.* **2019**, *52*, 356 – 366; d) X. F. Lu, P. Q. Liao, J. W. Wang, J. X. Wu, X. W. Chen, C. T. He, J. P. Zhang, G. R. Li, X. M. Chen, *J. Am. Chem. Soc.* **2016**, *138*, 8336 – 8339; e) J. Gascon, A. Corma, F. Kapteijn, F. X. Llabrés i Xamena, *ACS Catal.* **2014**, *4*, 361 – 378; f) L. Zeng, X. Guo, C. He, C. Duan, *ACS Catal.* **2016**, *6*, 7935 – 7947; g) M. Zhao, S. Ou, C. D. Wu, *Acc. Chem. Res.* **2014**, *47*, 1199 – 1207; h) L. Jiao, H. L. Jiang, *Chem* **2019**, *5*, 786 – 804.

[4] a) J. S. Qin, D. Y. Du, W. Guan, X. J. Bo, Y. F. Li, L. P. Guo, Z. M. Su, Y. Y. Wang, Y. Q. Lan, H. C. Zhou, *J. Am. Chem. Soc.* **2015**, *137*, 7169 – 7177; b) I. Hod, P. Deria, W. Bury, J. E. Mondloch, C. W. Kung, M. So, M. D. Sampson, A. W. Peters, C. P. Kubiak, O. K. Farha, J. T. Hupp, *Nat. Commun.* **2015**, *6*, 8304; c) M. Jahan, Z. Liu, K. P. Loh, *Adv. Funct. Mater.* **2013**, *23*, 5363 – 5372; d) D. Micheroni, G. Lan, W. Lin, *J. Am. Chem. Soc.* **2018**, *140*, 15591 – 15595; e) J. Duan, S. Chen, C. Zhao, *Nat. Commun.* **2017**, *8*, 15341; f) Y. P. Wu, W. Zhou, J. Zhao, W. W. Dong, Y. Q. Lan, D. S. Li, S. Sun, X. Bu, *Angew. Chem. Int. Ed.* **2017**, *56*, 13001 – 13005; *Angew. Chem.* **2017**, *129*, 13181 – 13185.

[5] S. Zhao, Y. Wang, J. Dong, C. T. He, H. Yin, P. An, K. Zhao, X. Zhang, C. Gao, L. Zhang, J. Lv, J. Wang, J. Zhang, A. M. Khattak, N. A. Khan, Z. Wei, J. Zhang, S. Liu, H. Zhao, Z. Tang, *Nat. Energy* **2016**, *1*, 16184.

[6] a) A. Agrawal, S. H. Cho, O. Zandi, S. Ghosh, R. W. Johns, D. J. Milliron, *Chem. Rev.* **2018**, *118*, 3121 – 3207; b) L. M. Liz-Marzán, C. J. Murphy, J. Wang, *Chem. Soc. Rev.* **2014**, *43*, 3820 – 3822; c) H. Yang, L. Q. He, Y. W. Hu, X. Lu, G. R. Li, B. Liu, B. Ren, Y. Tong, P. P. Fang, *Angew. Chem. Int. Ed.* **2015**, *54*, 11462 – 11466; *Angew. Chem.* **2015**, *127*, 11624 – 11628.

[7] a) C. Wang, X. G. Nie, Y. Shi, Y. Zhou, J. J. Xu, X. H. Xia, H. Y. Chen, *ACS Nano* **2017**, *11*, 5897 – 5905; b) P. V. Kamat, G. V. Hartland, *ACS Energy Lett.* **2018**, *3*, 1467 – 1469; c) Y. Shi, J. Wang, C. Wang, T. T. Zhai, W. J. Bao, J. J. Xu, X. H. Xia, H. Y. Chen, *J. Am. Chem. Soc.* **2015**, *137*, 7365 – 7370; d) G. Liu, P. Li, G. Zhao, X. Wang, J. Kong, H. Liu, H. Zhang, K. Chang, X. Meng, T. Kako, J. Ye, *J. Am. Chem. Soc.* **2016**, *138*, 9128 – 9136; e) C. Wang, Y. Shi, D. R. Yang, X. H. Xia, *Curr. Opin. Electrochem.* **2018**, *7*, 95 – 102.

[8] L. Liu, S. Ouyang, J. Ye, *Angew. Chem. Int. Ed.* **2013**, *52*, 6689 – 6693; *Angew. Chem.* **2013**, *125*, 6821 – 6825.

[9] H. X. Zhang, Y. Li, M. Y. Li, H. Zhang, J. Zhang, *Nanoscale* **2018**, *10*, 2236 – 2241.

[10] C. Kim, B. L. Suh, H. Yun, J. Kim, H. Lee, *ACS Catal.* **2017**, *7*, 2294 – 2302.

[11] S. Linic, U. Aslam, C. Boerigter, M. Morabito, *Nat. Mater.* **2015**, *14*, 567 – 576.

[12] Z. Li, J. D. Xiao, H. L. Jiang, *ACS Catal.* **2016**, *6*, 5359 – 5365.

[13] a) H. Cui, G. Zhu, Y. Xie, W. Zhao, C. Yang, T. Lin, H. Gu, F. Huang, *J. Mater. Chem. A* **2015**, *3*, 11830 – 11837; b) D. R. Baker, P. V. Kamat, *Adv. Funct. Mater.* **2009**, *19*, 805 – 811; c) Z. Xie, X. Liu, W. Wang, X. Wang, C. Liu, Q. Xie, Z. Li, Z. Zhang, *Nano Energy* **2015**, *11*, 400 – 408; d) J. Kamimura, P. Bogdanoff, M. Ramsteiner, P. Corfdir, F. Feix, L. Geelhaar, H. Riechert, *Nano Lett.* **2017**, *17*, 1529 – 1537; e) J. S. DuChene, G. Tagliabue, A. J. Welch, W. H. Cheng, H. A. Atwater, *Nano Lett.* **2018**, *18*, 2545 – 2550.

[14] H. H. Wei, Z. J. Yang, Y. L. Min, J. C. Fan, Q. J. Xu, *Part. Part. Syst. Charact.* **2017**, *14*, 1600200.

[15] a) D. E. Scaife, *Sol. Energy* **1980**, *25*, 41 – 54; b) N. Tian, Y. Zhang, X. Li, K. Xiao, X. Du, F. Dong, G. I. N. Waterhouse, T. Zhang, H. Huang, *Nano Energy* **2017**, *38*, 72 – 81.

Manuscript received: May 16, 2019
Accepted manuscript online: June 3, 2019
Version of record online: June 27, 2019

